Influence of laser contrast on high-order harmonic generation from solid-density plasma surfaces

Jian Gao (高 健)[1,2], Feng Liu (刘 峰)[1,2,*], Xulei Ge (葛绪雷)[1,2,3], Yanqing Deng (邓彦卿)[1,2,4], Guobo Zhang (张国博)[1,2,4], Yuan Fang (方 远)[1,2], Wenqing Wei (魏文青)[1,2], Su Yang (杨 骕)[1,2], Xiaohui Yuan (远晓辉)[1,2], Min Chen (陈 民)[1,2], Zhengming Sheng (盛政明)[1,2,5], and Jie Zhang (张 杰)[1,2]

[1]*Key Laboratory for Laser Plasmas (Ministry of Education) and Department of Physics and Astronomy, Shanghai Jiao Tong University, Shanghai 200240, China*

[2]*Collaborative Innovation Center of IFSA (CICIFSA), Shanghai Jiao Tong University, Shanghai 200240, China*

[3]*State Key Laboratory of Surface Physics and Department of Physics, Fudan University, Shanghai 200433, China*

[4]*College of Science, National University of Defense Technology, Changsha 410073, China*

[5]*SUPA, Department of Physics, University of Strathclyde, Glasgow G4 0NG, UK*

**Corresponding author: liuf001@sjtu.edu.cn*

Received December 22, 2016; accepted April 28, 2017; posted online May 15, 2017

The influence of laser temporal contrast on high-order harmonic generation from intense laser interactions with solid-density plasma surfaces is experimentally studied. A switchable plasma mirror system is set up to improve the contrast by two orders of magnitude at 10 ps prior to the main peak. By using the plasma mirror and tuning the prepulse, the dependence of high-order harmonic generation on laser contrast is investigated. Harmonics up to the 21st order via the mechanism of coherent wake emission are observed only when the targets are irradiated by high contrast laser pulses by applying the plasma mirror.

OCIS codes: 190.2620, 240.4350, 320.7110.

doi: 10.3788/COL201715.081902.

High-order harmonic generation (HOHG) from the interactions of relativistically intense laser pulses with solid-density plasma surfaces has been demonstrated as a promising bright coherent x-ray source in the last decade. In contrast with the harmonic generation from laser-gas interactions, whose pulse intensities are limited by the gas ionization threshold and poor phase matching at laser intensities beyond 10^{15} W/cm^2[1–4], the HOHG from solid targets has no limitation on laser intensities, so it can reach much higher pulse intensities to improve the conversion efficiency. Recently, it is further extended to the generation of intense isolated attosecond pulses[5,6] with near diffraction-limited spatial beam quality[7], which can be regarded as a powerful tool for diagnosing the properties of plasmas[8,9] and imaging science[10,11].

Since HOHG from solid targets was observed with a CO_2 laser for the first time by Carman *et al.* in 1981[12], it has been extensively investigated both experimentally[13–16] and theoretically[17–22]. Now there are two well-recognized mechanisms of HOHG from plasma surfaces distinguished by the laser intensities, coherent wake emission (CWE)[17–19], and relativistically oscillating mirror (ROM)[20–22]. The harmonics of the CWE dominate the emission at moderate laser intensities $a_0 < 1$, where $a_0 = eE/(m\omega_L c)$ is the normalized vector potential, e and m are the electron charge and mass, E and ω_L are the amplitude and frequency of the laser electric field, and c is the light velocity in a vacuum. The Brunel electrons[23] are pulled out and pushed back into overdense plasmas periodically by the driven laser and excite plasma oscillations. These oscillations coherently emit harmonics in the specular direction of the incident laser. In the CWE mechanism, the highest harmonic order $H_{\max}$ is restricted by the maximum electron density of the plasma $n_{\max}$ with $H_{\max} = \sqrt{n_{\max}/n_c}$, where n_c is the critical density. For the 800 nm laser, the $H_{\max}$ with different targets of CH ($n_{\max} = 225n_c$), fused silica ($n_{\max} = 400n_c$) and aluminum ($n_{\max} = 441n_c$) are 15, 20, and 21, respectively. At the relativistic laser intensities ($a_0 \geq 1$), the ROM mechanism dominates the radiation. In the ROM mechanism, the surface of the overdense plasma is driven to oscillate with moving velocity $\nu \approx c$ as a plasma mirror (PM). When the incident laser is reflected by this relativistically oscillating surface, harmonics are generated due to the Doppler shift effect. Baeva *et al.*[22] showed that the harmonics have a spectrum with a roll off as $I_H = H^{-8/3}$, where I_H and H are the intensity and the order of a given harmonic. The harmonic spectrum extends to the cutoff order $H_{\max} \sim 8^{1/2}\gamma_{\max}^3$, where $\gamma_{\max}$ is the maximal γ factor of the plasma surface, determined by the laser intensities.

Both in the CWE and the ROM processes, a very steep density gradient at the plasma-vacuum interface is needed for efficient harmonic generation. The density profile at the plasma surface of a solid target depends on the laser intensities and temporal contrast, so the temporal contrast of the incident laser pulse plays a crucial role in the HOHG. In this Letter, the influence of the driven laser contrast on the HOHG by the CWE mechanism is investigated experimentally by using a PM system to modify the laser contrast.

The experiment was carried out using the 200 TW Ti: sapphire laser system at the Laboratory for Laser Plasmas at Shanghai Jiao Tong University. The laser system can deliver laser pulses at 800 nm with energies on the target up to 5 J, pulse durations (full width at half-maximum, FWHM) of 25 fs, and repetition rates of 10 Hz.

The sketch of the experimental setup for the HOHG measurement is presented in Fig. 1. The laser beam with an energy of 1.7 J was used in the experiment and focused by an F/4 off-axis parabolic (OAP) mirror at an incidence angle of 15° to the target normal. The focal spot diameter was 6 μm (FWHM) with 25% energy enclosed, giving a calculated peak intensity of 6×10^{19} W/cm^2. Polished fused silica plates with a surface flatness of $\lambda/8$ at 632.8 nm were used as targets. The high-order harmonic radiations generated at the specular direction were collected by a gold toroidal mirror ($f = 490$ mm) at the entrance slit of a flat-field spectrometer (HORIBA JOBIN YVON, TGS300). The spectrometer consisted of a gold-coated toroidal grating and a back-illuminated x-ray CCD camera (Andor, Newton 940). An Al filter between the slit and the grating was used to block the reflected laser beam and transmit the harmonics in the spectral range from 17.1 to 80 nm.

The HOHG process is very sensitive to the plasma density gradient at the plasma surface, which is created by the amplified spontaneous emission (ASE) and leading edge of the laser pulse. Therefore, high contrast laser pulses are preferred for the HOHG. A single PM system had been set up to enhance the laser temporal contrast. The schematic of the PM system and the measured ASE contrasts are shown in Fig. 2. As shown in Fig. 2(a), the p-polarized laser pulse was focused by an F/10 OAP1 mirror at an incidence angle of 10° onto an antireflection-coated fused silica glass. The silica glass was mounted on a 3D motorized stage so it could provide a flesh surface for each shot. The laser intensity on the PM was properly set so that the ASE was low enough to transmit through the PM, while the leading edge of the main pulse was intense enough to

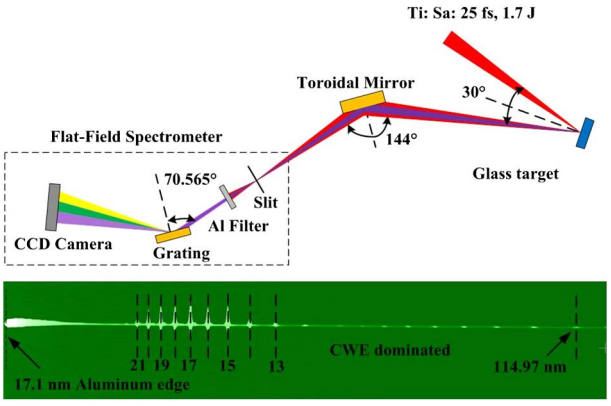

Fig. 1. Top panel is the experimental setup for HOHG. The bottom panel is the raw image of the harmonic spectrum obtained from the glass target with a PM.

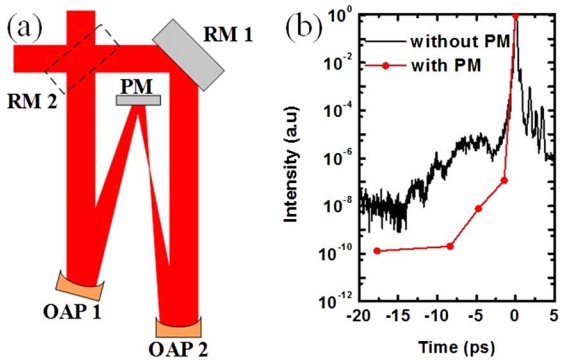

Fig. 2. (a) Schematic of the PM system. (b) The picosecond ASE contrast ratios measured without (black) and with (red) the PM.

ionize the PM, which could reflect the main pulse as a mirror. The reflected pulse was re-collimated by identical OAP2 mirror, which was further reflected by a reflective mirror 1 (RM1) to the target chamber. The RM2 could be moved into the beam path to bypass the PM system, providing laser pulses with lower contrast. The picosecond ASE contrasts were measured with a commercial third-order cross correlator (Sequoia, Amplitude Technologies). Figure 2(b) depicts the ASE contrasts measured with and without the PM. It is shown that the contrast at 10 ps prior to the main peak is improved 100 fold from ~10^{-8} to ~10^{-10} when the PM is used. The focused laser intensity on the target decreases to 3.5×10^{19} W/cm^2, when the PM reflectivity of 58% is taken into account.

The bottom panel in Fig. 1 shows a typical raw spectrum image of harmonics obtained by a single shot when the PM is used. The intensities of the 13th to 21st harmonics strongly saturate the CCD camera because a very thin Al filter, with a thickness of 250 nm, is used for this shot, but no harmonic with an order higher than 21st is observed. These are the characteristics of the harmonics generated by the CWE mechanism, whose highest harmonic order is limited by the maximum plasma density. In order to obtain the unsaturated spectra of the harmonics, another piece of Al filter, with a thickness of 1.5 μm, was put in the spectrometer to attenuate the intensities on the CCD. The spectra obtained with and without the PM are compared in Fig. 3. In Fig. 3(a), discrete harmonics from 17th to 21st orders and the Al L absorption edge at 17.1 nm are clearly observed when the PM is used. Figure 3(b) shows a spectrum obtained when the PM is not used by moving in RM2 to bypass the PM. No harmonic and only plasma emission is obtained when the PM is not used. The first, second, and third-order diffractions of the Al L absorption edge can be seen clearly corresponding to the wavelengths of 17.1, 34.2, and 51.3 nm, respectively. The normalized intensities of the spectra in Fig. 3 are calculated by taking into account the reflectance of the toroidal mirror and the grating, the transmittance of the Al filters, and the quantum efficiency of the CCD camera.

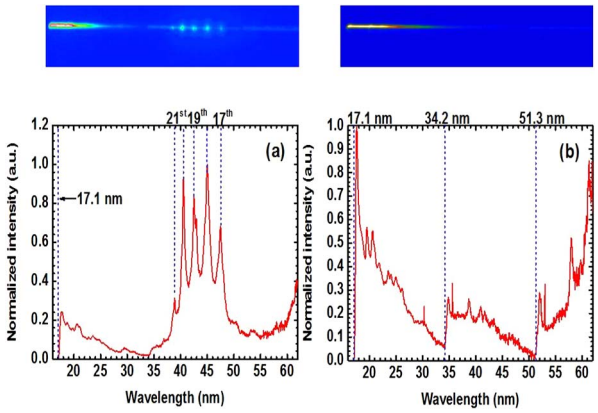

Fig. 3. The raw spectral image (top panel) and spectrum of high-order harmonics (bottom panel) obtained (a) with and (b) without the PM in the specular direction of the incident laser.

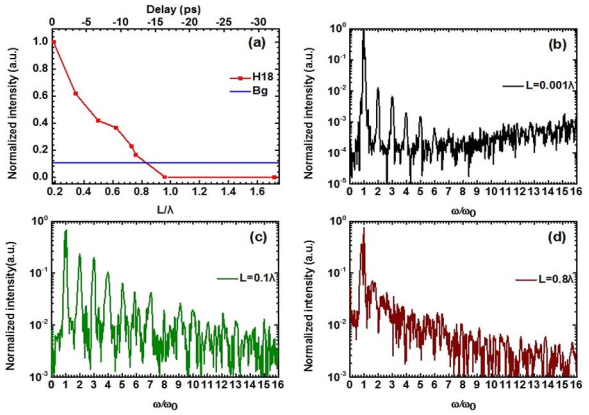

Fig. 4. (Color online) (a) Dependence of 18th harmonic intensities on the plasma scale lengths L obtained in the experiment (red). The blue line indicates the intensity of the background plasma emission. The harmonic spectra obtained by PIC simulations with different plasma scale lengths (b) $L = 0.001\lambda$ (black), (c) $L = 0.1\lambda$ (green), and (d) $L = 0.8\lambda$ (brown).

In the experiment, no harmonic with an order over the CWE cutoff at the 21st is observed. There are three possible reasons for the ROM harmonics not being generated, including the intensities, the temporal contrast, and the incidence angle of the laser. First, the normalized vector potential a_0 is the key parameter determining whether the harmonics are generated by the CWE or the ROM mechanism. The CWE harmonics dominate the radiation of nonrelativistic laser intensities with $a_0 < 1$, while the ROM harmonics dominate the radiation of relativistic laser intensities with $a_0 \geq 1$. However, the peak laser intensity when the PM is used in the experiment is 3.5×10^{19} W/cm^2 with corresponding $a_0 = 4$, which is beyond the relativistic intensity threshold. Second, it is verified both by numerical simulations[17,24] and experiments[25,26] that there is an optimum plasma scale length range L for the CWE or the ROM harmonic generation. When the plasma density is step-like L, both the CWE and the ROM could not be efficiently excited. The ROM requires a low-density plasma at the plasma surface, with $0.1\lambda_{\text{laser}} < L < \lambda_{\text{laser}}$. On the other hand, the CWE requires much steeper plasma, with $0 < L < 0.1\lambda_{\text{laser}}$. To change L, we introduce a prepulse with pulse duration (FWHM) of 50 fs and intensity of 2×10^{16} W/cm^2. L could be continuously tuned by varying the relative delay between the prepulse and the driven pulse from -33 to 3 ps. No ROM harmonic is observed, while the CWE harmonic intensities are found to decrease with increasing of the delay until they disappear after a delay of -12.33 ps. We use the hydrodynamic code MULTI to estimate L at different prepulse delays. The experimental data of the dependence of the 18th harmonic intensities on L are presented in Fig. 4(a). 2D particle-in-cell (PIC) simulations are also performed to obtain the HOHG spectra with three typical L, as shown in Figs. 4(b)–4(c), where a p-polarized laser field with an intensity of 3.5×10^{19} W/cm^2 ($a_0 = 4$) impinges on an overdense plasma with a maximum plasma electron density $400n_c$ with an incidence angle of 15°. From the simulation results, it can be clearly seen in Fig. 4(b) that the harmonic generation is not efficient for $L = 0.001\lambda_{\text{laser}}$. The harmonic intensities are enhanced dramatically up to $L = 0.1\lambda_{\text{laser}}$ in Fig. 4(c). However, if the scale length is further increased to $L = 0.8\lambda_{\text{laser}}$, no harmonics and only plasma emission could be seen in Fig. 4(d). In the CWE mechanism, the wake field cannot radiate efficiently if the plasma gradient is very steep ($L \sim 0$)[17,24,27]. On the other hand, the Brunel electrons that excite the wake field inside the plasma cannot be generated if the preplasma is too long[24,27]. The harmonic generation efficiency first increases very fast and then decreases slowly when L is increased, which agrees with the simulation results shown in Figs. 4(b)–4(d). In experiments, the laser leading edge always produces preplasma before the laser peak arriving at the target surface. The harmonic intensities show a monotonic decrease with the increase of L, as shown in Fig. 4(a). According to the above discussion, the laser intensities and contrast are ruled out for no ROM harmonic generation of our experiment. Finally, it is shown in Ref. [27] that the efficiency of HOHG reaches its maximum at an optimal incident angle of 55°. In our experiment, the incidence angle of the laser is 15°, which is much smaller than the optimal angle of 55°. In the future, we will increase the incidence angle to investigate its impact on the HOHG.

In conclusion, we find that in our experiment the temporal contrast of the incident laser is crucial for HOHG from plasma surfaces. A PM system is used to improve the ASE contrast of the laser by two orders of magnitude from $\sim 10^{-8}$ to $\sim 10^{-10}$ at 10 ps prior to the main peak. The harmonics up to the 21st order are observed from the solid plasma surface of the plain glass when the PM system is adopted, which is generated by the CWE mechanism. No harmonics and only plasma emission is obtained when the PM system is not used.

This work was supported by the National Basic Research Program of China (No. 2013CBA01502), the National Natural Science Foundation of China (Nos. 11305103, 11374209, 11374210, and 11205100), the Natural Science Foundation of Shanghai (No. 13ZR1456300), and the International Science & Technology Cooperation Program of China (No. 2014DFG02330).

References

1. J. L. Krause, K. J. Schafer, and K. C. Kulander, Phys. Rev. Lett. **68**, 3535 (1992).
2. P. B. Corkum, Phys. Rev. Lett. **71**, 1994 (1993).
3. C. Liu, P. Wei, J. Miao, C. Zhang, Y. Huang, Y. Zheng, Y. Leng, and Z. Zeng, Chin. Opt. Lett. **12**, 030201 (2014).
4. J. Jiang, P. Wei, Z. Zeng, X. Yuan, Y. Zheng, X. Ge, R. Li, and Z. Xu, Chin. Opt. Lett. **13**, 050202 (2015).
5. M. Yeung, J. Bierbach, E. Eckner, S. Rykovanov, S. Kuschel, A. Sävert, M. Förster, C. Rödel, G. G. Paulus, S. Cousens, M. Coughlan, B. Dromey, and M. Zepf, Phys. Rev. Lett. **115**, 193903 (2015).
6. H. Vincenti and F. Quéré, Phys. Rev. Lett. **108**, 113904 (2012).
7. B. Dromey, D. Adams, R. Hörlein, Y. Nomura, S. G. Rykovanov, D. C. Carroll, P. S. Foster, S. Kar, K. Markey, P. McKenna, D. Neely, M. Geissler, G. D. Tsakiris, and M. Zepf, Nat. Phys. **5**, 146 (2009).
8. U. Wagner, M. Tatarakis, A. Gopal, F. N. Beg, E. L. Clark, A. E. Dangor, R. G. Evans, M. G. Haines, S. P. D. Mangles, P. A. Norreys, M. S. Wei, M. Zepf, and K. Krushelnick, Phys. Rev. E. **70**, 026401 (2004).
9. A. Malvache, A. Borot, F. Quéré, and R. Lopez-Martens, Phys. Rev. E **87**, 035101 (2013).
10. R. L. Sandberg, A. Paul, D. A. Raymondson, S. Hädrich, D. M. Gaudiosi, J. Holtsnider, R. I. Tobey, O. Cohen, M. M. Murnane, and H. C. Kapteyn, Phys. Rev. Lett. **99**, 098103 (2007).
11. A. Ravasio, D. Gauthier, F. R. N. C. Maia, M. Billon, J. P. Caumes, D. Garzella, M. Géléoc, O. Gobert, J. F. Hergott, A. M. Pena, H. Perez, B. Carré, E. Bourhis, J. Gierak, A. Madouri, D. Mailly, B. Schiedt, M. Fajardo, J. Gautier, P. Zeitoun, P. H. Bucksbaum, J. Hajdu, and H. Merdji, Phys. Rev. Lett. **103**, 028104 (2009).
12. R. L. Carman, D. W. Forslund, and J. M. Kindel, Phys. Rev. Lett. **46**, 29 (1981).
13. P. A. Norreys, M. Zepf, S. Moustaizis, A. P. Fews, J. Zhang, P. Lee, M. Bakarezos, C. N. Danson, A. Dyson, P. Gibbon, P. Loukakos, D. Neely, F. N. Walsh, J. S. Wark, and A. E. Dangor, Phys. Rev. Lett. **76**, 1832 (1996).
14. J. Zhang, M. Zepf, P. A. Norreys, A. E. Dangor, M. Bakarezos, C. N. Danson, A. Dyson, A. P. Fews, P. Gibbon, M. H. Key, P. Lee, P. Loukakos, S. Moustaizis, D. Neely, F. N. Walsh, and J. S. Wark, Phys. Rev. A **54**, 1597 (1996).
15. B. Dromey, M. Zepf, A. Gopal, K. Lancaster, M. S. Wei, K. Krushelnick, M. Tatarakis, N. Vakakis, S. Moustaizis, R. Kodama, M. Tampo, C. Stoeckl, R. Clarke, H. Habara, D. Neely, S. Karsch, and P. Norreys, Nat. Phys. **2**, 456 (2006).
16. M. Bocoum, M. Thévenet, F. Böhle, B. Beaurepaire, A. Vernier, A. Jullien, J. Faure, and R. Lopez-Martens, Phys. Rev. Lett. **116**, 185001 (2016).
17. B. Dromey, S. G. Rykovanov, D. Adams, R. Hörlein, Y. Nomura, D. C. Carroll, P. S. Foster, S. Kar, K. Markey, P. McKenna, D. Neely, M. Geissler, G. D. Tsakiris, and M. Zepf, Phys. Rev. Lett. **102**, 225002 (2009).
18. B. Bezzerides, R. D. Jones, and D. W. Forslund, Phys. Rev. Lett. **49**, 202 (1982).
19. F. Quéré, C. Thaury, P. Monot, S. Dobosz, and P. Martin, Phys. Rev. Lett. **96**, 125004 (2006).
20. S. V. Bulanov, N. M. Naumova, and F. Pegoraro, Phys. Plasmas **1**, 745 (1994).
21. R. Lichters, J. Meyer-ter-Vehn, and A. Pukhov, Phys. Plasmas **3**, 3425 (1996).
22. T. Baeva, S. Gordienko, and A. Pukhov, Phys. Rev. E. **74**, 046404 (2006).
23. F. Brunel, Phys. Rev. Lett. **59**, 52 (1987).
24. K. Tarasevitch, C. Lobov, Wünsche, and D. von der Linde, Phys. Rev. Lett. **98**, 103902 (2007).
25. C. Rödel, D. van der Brügge, J. Bierbach, M. Yeung, T. Hahn, B. Dromey, S. Herzer, S. Fuchs, A. G. Pour, E. Eckner, M. Behmke, M. Cerchez, O. Jäckel, D. Hemmers, T. Toncian, M. C. Kaluza, A. Belyanin, G. Pretzler, O. Willi, A. Pukhov, M. Zepf, and G. G. Paulus, Phys. Rev. Lett. **109**, 125002 (2012).
26. S. Kahaly, S. Monchocé, H. Vincenti, T. Dzelzainis, B. Dromey, M. Zepf, P. Martin, and F. Quéré, Phys. Rev. Lett. **110**, 175001 (2013).
27. C. Thaury and F. Quéré, J. Phys. B **43**, 213001 (2010).